ELSEVIER

Physica D 159 (2001) 202–214

PHYSICA D

www.elsevier.com/locate/physd

Breathers in a single plaquette of Josephson junctions: existence, stability and resonances

A. Benabdallah*, M.V. Fistul, S. Flach

Max-Planck-Institut für Physik komplexer Systeme, Nöthnitzer Straße 38, D-01187 Dresden, Germany

Received 25 May 2001; accepted 24 July 2001
Communicated by A.C. Scott

Abstract

We present a theoretical study of *inhomogeneous* dynamic (resistive) states in a single plaquette consisting of three Josephson junctions. These breather states are found to exist in a large range of control parameters (d.c. bias γ, anisotropy η and self-inductance β_L). We perform an analytical analysis of these states, and their stability and resonance behaviour. Numerical calculations confirm our results and show that instabilities arise due to resonant interactions between the breather and electromagnetic oscillations (EOs) mediated by the breather state. These instabilities manifest themselves by various nonlinearities, resonant steps and voltage jumps in the current–voltage characteristics.

PACS: 05.45.−a; 05.45.Xt; 85.25.Cp

Keywords: Josephson junctions; Discrete breathers; Resonances

1. Introduction

In recent years, we witnessed a considerable advancing in the area of study of localized excitations in nonlinear lattices [1–3]. These excitations are coined discrete breathers and are time-periodic and spatially localized solutions of the underlying dynamical equations of motion. They generically appear in spatially homogeneous systems due to the interplay between discreteness and nonlinearity. Discrete breathers were detected experimentally in different systems, e.g. in weakly coupled optical waveguides [4], in the lattice dynamics of solids [5], in antiferromagnets [6] and in systems of interacting Josephson junctions [7–11].

Especially, the latter example served for many years as a well controlled laboratory object to study various nonlinear phenomena. Josephson junction systems allow for an adequate theoretical description of the underlying dynamics. The originally proposed and realized ladder geometry of small interacting Josephson junctions with an external d.c. bias became a system of intense theoretical and experimental studies [12–15]. The dynamic localized states in Josephson junction ladders persist due to a well-known property of a single Josephson junction, namely the presence of two different states. These are a superconducting state (SS) (zero voltage drop across the junction) or a resistive state (nonzero voltage drop across the junction). If the junction is underdamped, both states may coexist in a wide range of an externally applied d.c. bias. A well-known consequence of that is a hysteretic current–voltage (I–V) characteristics.

* Corresponding author.
E-mail address: abenab@mpipks-dresden.mpg.de (A. Benabdallah).

0167-2789/01/$ – see front matter
PII: S0167-2789(01)00338-4

A breather state in such a ladder is characterized by a few junctions being in the resistive state, while the rest of all junctions reside in the superconducting one. These inhomogeneous dynamic states lead to specific total d.c. voltage drops across the ladder which are used to plot I–V characteristics. This method has been successfully combined with snapshots made using the low temperature scanning laser microscopy (LTSM) technique which allows for a spatial resolution of d.c. voltage drops [8,9]. Note that the experimentally accessible information provides only with time-averaged data, so the internal dynamics of breather states is so far not directly observable in experiments. The full dynamical picture is, however, more subtle. For example, the superconducting junctions display nonzero a.c. voltage drops. The amplitude of these a.c. voltages decays to zero with increasing spatial distance from the resistive junctions. Moreover, a breather state may be tuned into resonance with other dynamical modes of the system which leads to an increasing complexity of the breather dynamics. Experimental studies revealed a whole "zoo" of different breather states, instabilities, resonances and switching scenarios depending on the parameters of the ladder [7–11]. Similar features have been found in numerical simulations.

To clarify the role of control parameters and the cause of the primary (generic) instabilities, resonances and switchings we carry out a consistent study of a *single plaquette model* containing three Josephson junctions. Whereas the occurrence of breathers in an extended ladder may be interpreted as a dynamical breaking of discrete translational invariance, in the single plaquette model, the analogy of the translational invariance becomes a permutational invariance. It is this permutational invariance which will be violated by dynamical states coined breathers in analogy to the ladder case. The approach of studying inhomogeneous dynamic states in reduced systems [15,16] has been successfully used in the past to get deeper understanding for different breather properties as, e.g. energy radiation and quantization [2].

Such a single plaquette model is the simplest system which supports permutationally broken states in the presence of a homogeneous d.c. bias γ (Fig. 1). It consists of two *vertical* Josephson junctions parallel to the bias direction and a *horizontal* one that is transversal to the bias. The Josephson junctions are indicated by crosses. In a time-averaged picture, we expect only four different states to be realized. The first one is characterized by all junctions being in the SS, with zero current flowing through the horizontal junction. The second one is the homogeneous whirling state (HWS) when both vertical junctions are in the resistive state. Due to permutational invariance of this state the current flowing through the superconducting horizontal junction is still zero. Note that both states are invariant under permutation, i.e. the exchange of two vertical junctions. The states of interest are the remaining two breather states. Each of these states is characterized by only one vertical junction and in addition the horizontal junction being resistive. The second vertical junction is in an SS, although there is a nonzero current flowing through it. Obviously, both breather states are not invariant under permutation.

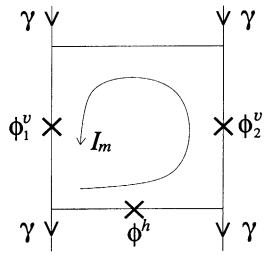

Fig. 1. Sketch of the plaquette with three Josephson junctions (marked by crosses) in the presence of uniform d.c. bias. Arrows indicate the direction of external current flow (d.c. bias γ).

In the following, we will systematically study the dependence of breather state properties on the control parameters of the system (d.c. bias, anisotropy, self-inductance). Our paper is organized in the following way. In Section 2, we present the model, introduce the equations of motion and provide with an approximative analytical treatment. In Section 3, we introduce a number of numerical methods for computing breathers, obtaining their stability and following their evolution. With their help, we find the domains of existence, stability and resonances of breather states in the space of control parameters and relate them to computed I–V characteristics.

2. Equations of motion and properties of breather solutions

2.1. Equations of motion

The dynamics of a single plaquette of three Josephson junctions (see Fig. 1) is determined by the time dependent Josephson phases of vertical junctions $\phi^{\mathrm{v}}_{1,2}$, and the horizontal junction ϕ^{h}. We will consider an anisotropic system and the parameter of anisotropy is $\eta = I_{\mathrm{ch}}/I_{\mathrm{cv}}$, where I_{ch} and I_{cv} are, respectively, the critical currents of the horizontal and vertical junctions. By making use of the *resistive shunted junction* model for each junction [17], we obtain the following set of equations:

$$\mathcal{N}(\phi^{\mathrm{v}}_1) = \gamma + I_{\mathrm{m}}, \qquad \mathcal{N}(\phi^{\mathrm{v}}_2) = \gamma - I_{\mathrm{m}},$$
$$\mathcal{N}(\phi^{\mathrm{h}}) = \frac{I_{\mathrm{m}}}{\eta}. \tag{1}$$

The nonlinear operator $\mathcal{N}$ is defined as

$$\mathcal{N}(\phi) = \ddot{\phi} + \alpha\dot{\phi} + \sin(\phi). \tag{2}$$

Here, the unit of time is the inverse plasma frequency, the d.c. bias γ is normalized to the critical current of the vertical junctions I_{cv}, and the dimensionless parameter α determines the damping in the system. In (1), we introduce the mesh current I_{m} that in turn, is determined by the flux quantization law [18]

$$-\beta_L I_{\mathrm{m}} = \phi^{\mathrm{v}}_1 - \phi^{\mathrm{v}}_2 + \phi^{\mathrm{h}}, \tag{3}$$

where $\beta_L = 2\pi I_{\mathrm{cv}} L/\Phi_0$ is the normalized self-inductance L of the plaquette. Note here that the voltage drop across a junction is given by $\dot{\phi}$.

2.2. Breather solutions

We are interested in the properties of inhomogeneous breather states. In the limit $\eta = 0$, we may exactly solve the equations of motion and implicitly obtain the breather solution in terms of the resistive state of a single vertical junction. In this case, the mesh current vanishes ($I_{\mathrm{m}} = 0$) and the two vertical junctions decouple, while the horizontal one follows the dynamics of the vertical junctions (below, we will consider a particular breather case as the left vertical junction is in the SS):

$$\phi^{\mathrm{v}}_1 = \arcsin\gamma, \qquad \phi^{\mathrm{v}}_2 = f(\alpha,\gamma,t),$$
$$\phi^{\mathrm{h}} = f(\alpha,\gamma,t) - \arcsin\gamma. \tag{4}$$

Here, the function $f(\alpha,\gamma,t)$ describes the evolution of a single vertical junction in the resistive state with bias γ and damping α. It is well known that this state exists as [17]

$$\gamma \geq \gamma_{\mathrm{r}} = \frac{4\alpha}{\pi}, \tag{5}$$

where γ_{r} is the retrapping current of a single Josephson junction. On the other side, the SS of the first vertical junction (see Eq. (4)) will persist only if $\gamma < 1$. Consequently, we obtain that the breather solution (4) exists for $\eta = 0$ provided $\gamma_{\mathrm{r}} \leq \gamma \leq 1$.

For nonzero values of $\eta \neq 0$, exact analytical solutions are not available. In the following, we obtain approximate solutions using a *d.c. analysis*, i.e. neglecting the Josephson phase oscillations. We write the Josephson phases in the form

$$\phi^{\mathrm{v}}_1 \approx c^{\mathrm{v}}_1, \quad \phi^{\mathrm{v}}_2 \approx \Omega t + c^{\mathrm{v}}_2, \quad \phi^{\mathrm{h}} \approx \Omega t + c^{\mathrm{h}}, \tag{6}$$

where Ω is the *breather frequency*. Substituting these expressions into (1) and (3), the mesh current reads

$$I_{\mathrm{m}} = \frac{\gamma\eta}{1+\eta}. \tag{7}$$

Correspondingly, the d.c. bias dependent breather frequency and the Josephson phase shifts are

$$\Omega = \frac{\gamma}{\alpha(1+\eta)}, \tag{8}$$

$$c^{\mathrm{v}}_1 = \arcsin\left(\frac{1+2\eta}{1+\eta}\gamma\right), \tag{9}$$

$$c^{\mathrm{v}}_2 = c^{\mathrm{v}}_1 + \frac{\beta_L\gamma\eta}{1+\eta}. \tag{10}$$

Here, we may choose $c^{\mathrm{h}} = 0$ without loss of generality. As a result, we find the I–V characteristics of the Josephson junction plaquette in the presence of a breather state

$$\gamma = V\alpha(1+\eta), \tag{11}$$

where $V = \langle \dot{\phi}_2^{\mathrm{v}} \rangle = \lim_{t\to\infty}(1/t)(\phi_2^{\mathrm{v}}(t) - \phi_2^{\mathrm{v}}(0))$. The I–V characteristics of a breather (11) differs from that of the HWS which is $\gamma = V\alpha$. The breather is characterized by a smaller voltage drop across the resistive vertical junction for a given current value γ.

As the d.c. bias current decreases, the breather state can disappear as a solution of the dynamic equations and the system undergoes a transition to the SS. By making use of the d.c. analysis and a standard theory of the retrapping current in a single small Josephson junction [17], we expect that the breather state disappears as the current flowing through the horizontal (resistive) junction is equal to γ_{r}. This happens for the following value of the external d.c. bias $\gamma_{\mathrm{b,r}}$:

$$\gamma_{\mathrm{b,r}} = \alpha(1+\eta)\frac{4}{\pi}. \tag{12}$$

Remarkably, this value of the retrapping current does not depend on the self-inductance parameter β_L. The dependence of $\gamma_{\mathrm{b,r}}$ on η is shown in Fig. 2.

For large values of the d.c. bias the breather state *switches* to the HWS. This switching occurs because the left vertical junction cannot anymore support the SS. From (9), we obtain that this switch should take place at

$$\gamma = \frac{1+\eta}{1+2\eta}. \tag{13}$$

The crucial assumption of the above carried out analysis is the neglecting of the Josephson phase oscillations. Indeed, the inhomogeneous dynamic breather state induces the electromagnetic oscillations (EOs) in the plaquette and in turn, these EOs change the simple breather solution (6). However, if the breather frequency Ω is large with respect to the characteristic frequencies of EOs, the influence of such a *nonresonant* interaction between the breather and EOs is small. Thus, in the nonresonant case the amplitude A of the breather induced EOs is $A \simeq \sqrt{2}\eta/(2\eta+1)\Omega^2$ and correspondingly, it leads to a corrected prediction of the critical d.c. bias value $\gamma_{\mathrm{b,HWS}}$, where the breather switches to the HWS:

$$\gamma_{\mathrm{b,HWS}} = \frac{1+\eta}{1+2\eta}\left(1 - \frac{\eta^2(2\eta+1)^2\alpha^4}{2}\right). \tag{14}$$

The result is shown in Fig. 2. Note that similar existence regions for the breathers on extended ladder have been reported in [10].

The main outcome of the presented analytical treatment is a triangular shaped region in the space of control parameters γ and η, where we expect to find breather states. Notably, the prediction is that for small values of damping ($\alpha \ll 1$), the breather should exist for rather large values of the anisotropy η, e.g. for $\alpha = 0.05$, the anisotropy can be as large as $\eta \sim 5$. Such parameter regions are the opposite of what has been initially anticipated, when the breather states were found by making use of the continuation arguments for the solution (4) at $\eta = 0$ to small nonzero η values [19]. In this case, the horizontal junctions serve as weak links. Instead, we predict the existence of breather states for cases of large η values where the vertical junctions serve as weak links, and the horizontal one is a strong link!

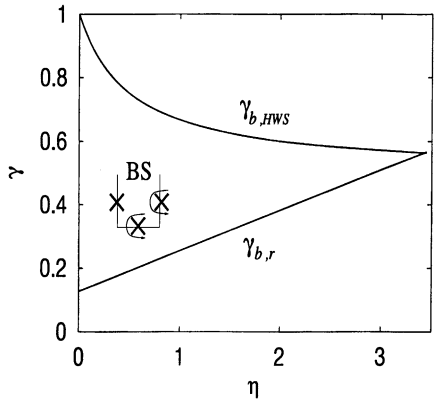

Fig. 2. Analytic boundaries of the breathers existence in (γ, η) plane for $\beta_L = 0$, $\alpha = 0.1$. The d.c. analysis was used.

2.3. EO frequencies and resonances

Next, we turn to the analysis of the *resonant interaction* between the breather state and small amplitude EOs. In order to obtain the characteristic frequencies of EOs, we linearize the dynamic equations around the breather state (6):

$$\ddot{\delta}_1^{\mathrm{v}} + \alpha\dot{\delta}_1^{\mathrm{v}} + \cos(c_1^{\mathrm{v}})\delta_1^{\mathrm{v}} = -\frac{1}{\beta_L}(\delta_1^{\mathrm{v}} - \delta_2^{\mathrm{v}} + \delta^{\mathrm{h}}), \tag{15}$$

$$\ddot{\delta}_2^{\mathrm{v}} + \alpha\dot{\delta}_2^{\mathrm{v}} + \cos(\Omega t + c_2^{\mathrm{v}})\delta_2^{\mathrm{v}} = \frac{1}{\beta_L}(\delta_1^{\mathrm{v}} - \delta_2^{\mathrm{v}} + \delta^{\mathrm{h}}), \tag{16}$$

$$\ddot{\delta}^{\mathrm{h}} + \alpha\dot{\delta}^{\mathrm{h}} + \cos(\Omega t)\delta^{\mathrm{h}} = -\frac{1}{\eta\beta_L}(\delta_1^{\mathrm{v}} - \delta_2^{\mathrm{v}} + \delta^{\mathrm{h}}). \tag{17}$$

Here $\delta_{1,2}^{\mathrm{v}}(t)$, $\delta^{\mathrm{h}}(t)$ correspond to small amplitude EOs excited in the presence of the breather state. In the weakly damped case ($\alpha \ll 1$), we may neglect the damping term and skip the time-periodic terms in (16) and (17). As a result, we derive two characteristic frequencies of EOs:

$$|\omega_{\pm}| = \sqrt{F \pm \sqrt{F^2 - G}}, \tag{18}$$

$$F = \frac{1}{2}\cos(c_1^{\mathrm{v}}) + \frac{1+2\eta}{2\eta\beta_L}, \tag{19}$$

$$G = \cos(c_1^{\mathrm{v}})\frac{1+\eta}{\eta\beta_L}. \tag{20}$$

These frequencies depend on the anisotropy η and the bias current through the phase shift c_1^{v} (Eq. (9)). For large values of β_L, the lower frequency $\omega_- \sim 1/\sqrt{\beta_L}$ and the large frequency $\omega_+ \sim \sqrt{\cos(c_1^{\mathrm{v}})}$. In the opposite limit of small β_L, we find $\omega_+ \sim 1/\sqrt{\beta_L}$, while $\omega_- \sim [((1+\eta)/(1+2\eta))^2 - \gamma^2]^{1/4}$.

Since the breather is a time-periodic solution and the EOs describe small amplitude deviations from the breather state, we can expect that the following scenario holds. In the case of a proper frequency matching, the breather may drive EOs into resonance. In turn, the increase in the EO amplitudes will proceed on the expense of the breather state. In other words, the possibility of a breather mediated resonance for EOs turns into a resonant interaction between the breather and the EOs. In such a case, we expect in the full dynamical system various instabilities of the breather state and corresponding switchings (the voltage jumps) or *resonant steps* in the I–V characteristics to occur.

Let us classify the possible expected resonance cases. The first class of *primary* resonances may appear if

$$\omega_{\pm} = m\Omega, \tag{21}$$

where m is an integer. These primary resonances correspond to a matching of the breather frequency Ω or its multiples (higher harmonics of the breather state) with the EOs frequencies.

A second class consists of *parametric* resonances which are characterized by

$$\omega_{\pm} = (m + \tfrac{1}{2})\Omega. \tag{22}$$

Finally, we may also expect the appearance of *combination* resonances occurring as

$$m\Omega = \omega_- \pm \omega_+. \tag{23}$$

In such a case, which is at variance with the first two types of resonances, the breather mediates a resonant interaction between two different EO frequencies.

All listed scenarios of resonance involve the breather frequency and the EO frequencies. While the approximate expression for the breather frequency (8) is *independent* on β_L, the EO frequencies *depend* sensitively on the self-inductance (18). Consequently, the expected positions of resonances vary with β_L. Since the existence window for breathers (cf. Fig. 2) is expected not to depend on β_L, certain resonances may simply be shifted outside the breather existence region and thus, become irrelevant. For example, for small values of β_L, the EO frequency ω_+ becomes very large and we expect then only primary and parametric resonances involving ω_-. If, however, intermediate values for β_L are chosen, additional primary and parametric resonances involving ω_+ appear. But most important, we expect combination resonances to appear, which can be realized only if the two EO frequencies, their sum or difference are of the same order as the breather frequency.

3. Numerical analysis of breather dynamics

3.1. Description of numerical methods

Let us describe the numerical methods of monitoring and characterizing breather states. In all cases a Runge–Kutta integration method of the differential equations (1) is chosen. The first way is to fix all parameters including the bias γ, to choose some proper initial conditions and to integrate the equations for

sufficiently long time until the system relaxes onto a breather attractor. Once the attractor is reached (with sufficient accuracy), all characteristics of this state may be obtained, including the average voltage drop V. After that we may perform a small step in γ and repeat the procedure. Then, we find the I–V characteristics. This method is especially good when approaching an instability, since we obtain explicitly the switching to another state. We also generate time-resolved images (movies) of the full dynamical behaviour in order to visually check the realized state or monitor the process of switching. The drawback of this method is that it is not capable of explaining the nature of an observed instability. In addition, it may become time consuming if the relaxation time becomes large.

Another way of studying the system states is to use a Newton scheme that allows to iteratively find time-periodic states, e.g. breathers. This method is very fast and possesses a high precision. Once a solution is found, it may be characterized similar to the way described above. The drawback here is that we cannot predict the outcome of a switching if a breather state disappears or turns unstable. The method is even insensitive to the stability property of a state under consideration, so we may even miss the switching.

In order to obtain reliable information about the stability properties of breather states, we perform in addition a Floquet analysis of small amplitude deviations from a breather state which we generated with the help of a Newton scheme. We consider the time evolution of small perturbations $\{\epsilon_i(0), \dot{\epsilon}_i(0)\}$ $(i = 1, 2, 3)$ at $t = 0$ of a breather solution $(\phi^{\mathrm{v}}_{1,2}, \phi^{\mathrm{h}})$ over one period T_{b} of the breather state. The outcome is a map of the space of small perturbations onto itself, which is characterized by a Floquet matrix $\mathcal{M}$ (of rank 6):

$$\begin{Bmatrix} \epsilon_i(T_{\mathrm{b}}) \\ \dot{\epsilon}_i(T_{\mathrm{b}}) \end{Bmatrix} = \mathcal{M} \begin{Bmatrix} \epsilon_i(0) \\ \dot{\epsilon}_i(0) \end{Bmatrix}. \tag{24}$$

This matrix is generated numerically. The breather will be linearly stable if and only if the matrix $\mathcal{M}$ has no eigenvalues with modulus larger than 1. The quasi-symplectic properties of this map impose the following conditions on its eigenvalues: if λ is an eigenvalue, then λ^*, $\mathrm{e}^{-\alpha T_{\mathrm{b}}}/\lambda$ and $\mathrm{e}^{-\alpha T_{\mathrm{b}}}/\lambda^*$ are also eigenvalues (here a^* denotes complex conjugation of a) [20]. Furthermore, there is always one eigenvalue $\lambda_t = 1$ which corresponds to perturbations tangent to the trajectory of the breather solution. Consequently, there always exists a second eigenvalue $\tilde{\lambda}_t = \mathrm{e}^{-\alpha T_{\mathrm{b}}}$. These two eigenvalues will not be of further interest. The remaining four eigenvalues can be grouped into two pairs each consisting of an eigenvalue and its complex conjugated partner. These two groups correspond to the two EO frequencies (18). In the normal case of a stable breather, two eigenvalues are simply characterized by

$$\lambda^{\pm} = \mathrm{e}^{-\alpha T_{\mathrm{b}}/2}\, \mathrm{e}^{\mathrm{i}\omega_{\pm} T_{\mathrm{b}}}. \tag{25}$$

Thus the four relevant eigenvalues will be located on an inner circle with radius $\mathrm{e}^{-\alpha T_{\mathrm{b}}/2} < 1$ in the complex plane. The variation of parameters system leads to a change (moving) of Floquet eigenvalues. Resonances correspond to collisions of an eigenvalue with its complex conjugated partner on the positive real axis (primary resonance), on the negative real axis (parametric resonance) or to the collision of two different eigenvalues away from the real axis (combination resonance). In all cases, colliding eigenvalues will generally leave the inner circle, one moving inside and one outside. Upon further variation of some parameter, the outer one may cross the unit circle, which marks the point of instability of the breather state. For small values of α, the two events — collision and crossing the unit circle — take place close to each other, so that a clear connection between instabilities and resonances may be drawn. The Floquet analysis thus allows in addition to characterize the type of observed instability (resonance).

A combination of all three methods — direct numerical integration, Newton scheme and Floquet analysis — turns out to be a powerful tool which provides good insight of the dynamical processes under consideration.

3.2. Domains of breather existence and instability windows

In order to obtain the breather solution for different values of anisotropy η and correspondingly, the

domains of breather existence in the parameter space (γ, η), we used the following procedure. First, we fixed the value of the external d.c. bias γ and found a breather solution in the form (4). After that we increased the parameter η by a small step $\Delta\eta = 10^{-2}$, and the previously found solution was used as an initial guess for a Newton method. The procedure was repeated for other values of d.c. bias γ. We varied the self-inductance parameter β_L, while in most of our simulations the damping parameter $\alpha = 0.1$ was fixed.

3.2.1. Zero self-inductance case ($\beta_L = 0$)

In the particular case of zero self-inductance β_L, Eq. (1) is simplified as $\phi^{\mathrm{h}} = \phi_1^{\mathrm{v}} - \phi_2^{\mathrm{v}}$, and the system is characterized by just two degrees of freedom. We found that the domains of breather existence in the parameter space γ–η have a triangular form, and it is shown in Fig. 3.

One can also see that the existence domain expands in the region of large η as the damping parameter α decreases (Fig. 3a and b). The maximum value of the anisotropy $\eta_{\max}$ still allowing to obtain the breather state is estimated as $\eta_{\max} \simeq 1/4\alpha$ (see inset in Fig. 3b). Note here, as the anisotropy is not large ($\eta \leq 1.5$ for the system with damping $\alpha = 0.1$), the d.c. analysis developed in Section 2 (see Fig. 2 and Eqs. (12) and (13)) gives a good approximation for numerically simulated domain of breather existence (Fig. 3). As the anisotropy increases, $\eta > 1$, the region of d.c. bias γ, where the breather state was found, shrinks with respect to the one obtained by making use of the d.c. analysis.

In order to study the interaction of the breather state with EOs, we carried out direct numerical simulations of the system of Eqs. (1) and (3) for different values of anisotropy. Moreover, we monitored the current–voltage (I–V) characteristics of the system decreasing (increasing) the d.c. bias by a step of $\Delta\gamma = 0.0005$.[1] The initial values of the d.c. bias γ corresponded approximately to the centre of the breather existence domain for the particular value of the anisotropy η.

[1] As it was observed in Ref. [21] for the Josephson ladder case, tiny steps $\Delta\gamma$ and large integration times have to be used in order to observe various switchings in the I–V curves.

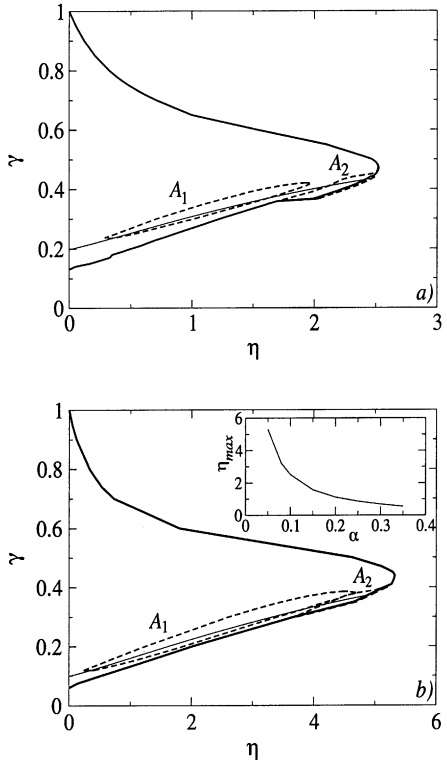

Fig. 3. Numerically obtained domains of breather existence (thick solid line) and instability windows (dashed) lines in parameter space (γ, η). The prediction of the breather state instability based on the parametric resonance between the breather state and EOs (Eq. (22) for $m = 0$) is shown by the thin solid line. The self-inductance $\beta_L = 0$, and the damping α is 0.1 (a) and 0.05 (b). The inset in (b) shows the dependence of the maximum value of anisotropy $\eta_{\max}$ on the damping α.

We start with the case of a small anisotropy $\eta = 0.1$ (Fig. 4). The breather was excited at $\gamma = 0.5$ and it persists in a wide range of the d.c. bias. The breather state *switches* to the HWS as γ increases beyond some critical value, and smoothly transits to the SS as the d.c. bias approaches the retrapping current (Eq. (12)). Note here that for such small values of anisotropy, the d.c. analysis (Eq. (11) and dashed line in Fig. 4) gives a good approximation practically for a whole I–V curve and it means that the resonant interaction of the breather with EOs is very weak.

As we increase the value of anisotropy to $\eta = 1$, the I–V curve displays peculiar features (Fig. 5). Indeed, as the d.c. bias decreases the I–V curve

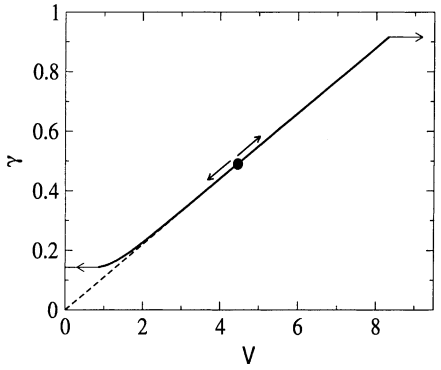

Fig. 4. I–V characteristics of a breather state for $\beta_L = 0$, $\alpha = 0.1$ and $\eta = 0.1$. The I–V curve obtained by making use of the d.c. analysis (dashed line) is also presented. The point indicates the initial value of d.c. bias and the arrows shows the process of d.c. bias increase (decrease).

deviates from the linear behaviour (Eq. (11) and dashed line in Fig. 5), displays a cusp at $\gamma = 0.34$ and eventually switches to the HWS state. It is interesting that this scenario is realized if we start from rather large values of the d.c. bias $\gamma \geq 0.33$. For lower d.c. bias values, we observe a second disconnected branch (the initial value of d.c. bias was 0.27) which displays a back bending and switching to the HWS in the I–V curve as the d.c. bias was increased. With decreasing current, this breather state transits to the SS.

All these features occurring in the current region $0.28 \leq \gamma \leq 0.33$ can be explained as a *parametric resonant interaction* between the breather state and excited EOs. First, we found a good agreement between the breather frequency $\Omega = \gamma/\alpha(1+\eta) = 1.6$ and the frequency of EOs, $2\omega_- = 1.52$ (for $\gamma = 0.32$). To study this resonant interaction more precisely, we carried out the Floquet analysis of the breather state. Fig. 6 illustrates the evolution of the modulus and the argument of the eigenvalues of the Floquet matrix $\mathcal{M}$ with γ. The arguments of the eigenvalues can be restricted as $0 \leq \mathrm{Arg}(\lambda) \leq \pi$. As the d.c. bias decreases, we observed that for the particular d.c. bias, $\gamma = 0.34$ an eigenvalue of the Floquet matrix crosses the unit circle at -1 (Fig. 6). Thus, the original breather state becomes *unstable* (although it continues to exist as a solution of the equations of motion) and this instability is driven by the parametric resonance (Fig. 6b) with the EO of the frequency ω_-. Note that as the current decreases further this eigenvalue returns into the unit

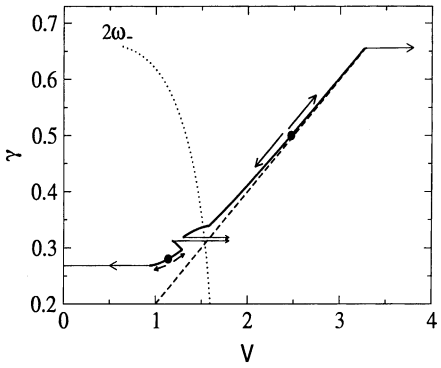

Fig. 5. I–V characteristics of a breather state for $\beta_L = 0$, $\alpha = 0.1$ and $\eta = 1$. The dotted line shows the dependence of the characteristic frequency combination of EOs on the d.c. bias γ and the dashed line represent the d.c. analysis.

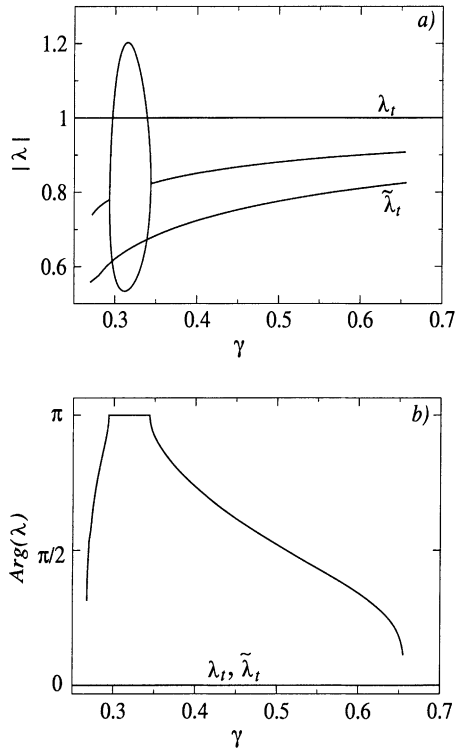

Fig. 6. (a) Modulus and (b) argument of the Floquet multipliers as a function of d.c. bias γ. The parameters are $\beta_L = 0$, $\alpha = 0.1$ and $\eta = 1$.

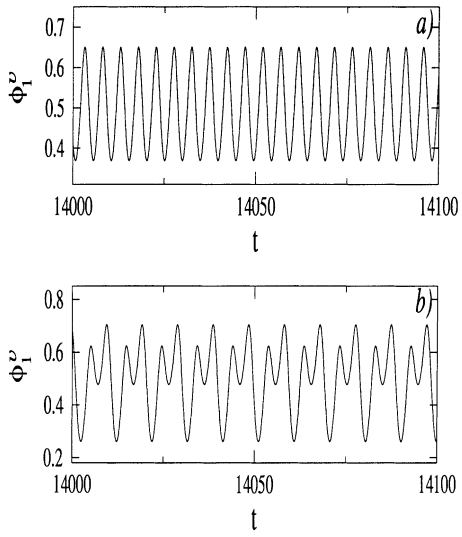

Fig. 7. Time dependence of the phase $\phi_1^{\mathrm{v}}(t)$ for two different values of d.c. bias: (a) $\gamma = 0.2965$; (b) $\gamma = 0.2970$. The parameters are $\beta_L = 0$, $\alpha = 0.1$ and $\eta = 1$.

circle, the breather state is again stable and thus an *instability window* of the breather is found (the region A_1 in Fig. 3a and b). The position of this instability window in the parameter space γ–η can be predicted using Eq. (22) or in the form (thin solid lines in Fig. 3):

$$\gamma_{\mathrm{m}}^{\mathrm{inst}}(\eta) = \frac{2\sqrt{2}\alpha^2(1+\eta)^2}{(2m+1)^2} \times \sqrt{-1+\sqrt{1+\frac{(2m+1)^4}{4\alpha^4(1+\eta)^2(1+2\eta)^2}}}. \tag{26}$$

The appearance of parametric resonance is often accompanied by a *period doubling* of the state mediating the resonance, and thus we checked the time dependence of the Josephson phase $\phi_1^{\mathrm{v}}(t)$. The results for two different d.c. bias values are presented in Fig. 7. One can see that for the d.c. bias $\gamma = 0.2965$, the period of the Josephson phase $\phi_1^{\mathrm{v}}(t)$ is two times less than the period of $\phi_1^{\mathrm{v}}(t)$ for the slightly larger value of $\gamma = 0.2970$. Thus, the "back bending" (and in same manner the "cusp") of the I–V curve (Fig. 5) is related to this period doubling process.

As the anisotropy η increases and approaches the tip of the domain of breather existence (Fig. 3), the

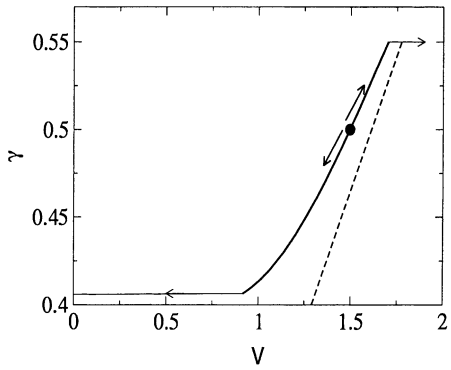

Fig. 8. I–V characteristics of a breather state for $\beta_L = 0$, $\alpha = 0.1$ and $\eta = 2.1$. The dashed line represents the d.c. analysis.

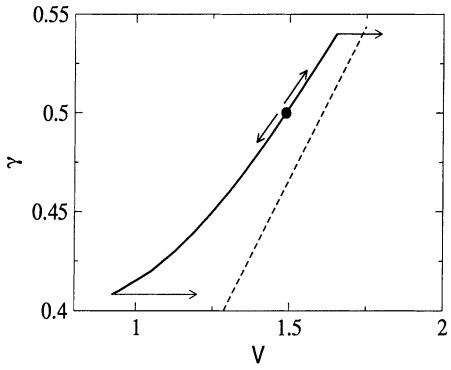

Fig. 9. I–V characteristics of a breather state for $\beta_L = 0$, $\alpha = 0.1$ and $\eta = 2.11$. The dashed line represents the d.c. analysis.

I–V characteristics start to display different features. First, for such a large value of anisotropy ($\eta \geq 2$), we observed a large deviation from the d.c. analysis (Figs. 8–10). It indicates a strong increase of the amplitudes of EOs. Presumably, this is also the reason why the switching to the HWS occurs for considerably smaller γ values as compared with the d.c. analysis. [2] This circumstance leads to a shrinking of the domain of breather existence at the tip.

We also found that the switching outcome in this region of anisotropy upon lowering the d.c. bias γ crucially depends on η. Indeed, for $\eta = 2.1$, we observed

[2] A similar effect of *external* a.c. force induced escape of Josephson phase has been analysed and experimentally observed by Fistul and Ustinov [22].

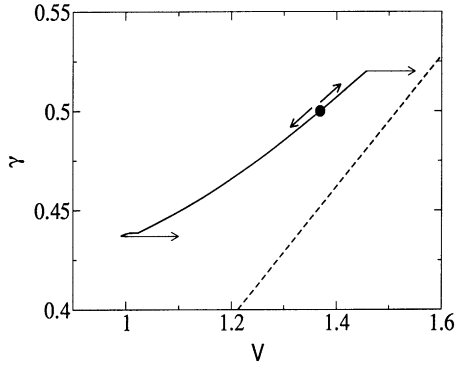

Fig. 10. I–V characteristics of a breather state for $\beta_L = 0$, $\alpha = 0.1$ and $\eta = 2.3$. The dashed line represents the d.c. analysis.

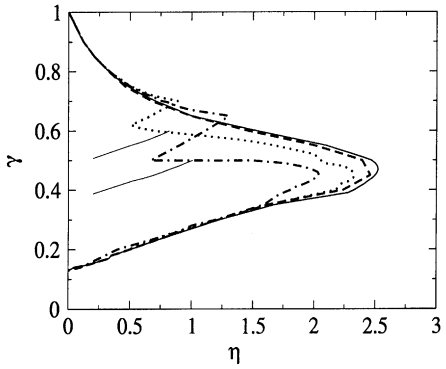

Fig. 11. Numerically simulated domains of breather existence in parameter space (γ, η) for: $\beta_L = 0$ (solid line), $\beta_L = 0.1$ (dashed line), $\beta_L = 0.3$ (dotted line) and $\beta_L = 0.5$ (dot-dashed line). The predicted resonances between the breather state and EOs, $\Omega = \omega_+$ for $\beta = 0.3$ and $\beta = 0.5$ (from top to bottom) are shown by the thin solid lines. The damping α is 0.1.

the switching to the SS (Fig. 8), but the breather state switches to the HWS (Fig. 9) as the parameter η becomes slightly above the value 2.11. Moreover, for $\eta = 2.3$ (Fig. 10), we observed that the switching to the HWS occurs via a peculiar intermediate state. This state is not periodic anymore (either quasiperiodic or chaotic in time), yet it shows up with typical breather features when averaged over time. It was stable over the whole simulation time of 10^6.

We carried out the Floquet analysis of the breather state and found the instability region (region A_2 in Fig. 3) that is also due to the parametric resonance between the breather state and EOs. At variance with the above considered instability window A_1, this instability region adjoins the lower boundary of the breather existence domain.

3.2.2. *Finite self-inductance case ($\beta_L \neq 0$)*

The breather properties depend crucially on the self-inductance parameter β_L. First, we found that the domain of the breather existence shrinks for small and moderate values of β_L (see Fig. 11).

Moreover, the upper boundary of the breather existence domain displays a "sawtooth" form for moderate values of the anisotropy ($\eta > 0.5$, see Fig. 11). The reason for such a peculiar shape of the breather existence domain is the resonant interaction between the breather state and EOs (thin solid lines in Fig. 11) leading to large amplitudes of EOs and corresponding a.c. induced instabilities of the SS of the left vertical junction. As the parameter β_L increases to large values (see Fig. 12), the resonant interaction between the breather state and EOs becomes weak again. In this case, the domain of breather existence practically coincides with the analytical predictions in Section 2 (see Fig. 2).

Also, similar to the case of $\beta_L = 0$, we found various instabilities of the breather state driven by the resonant interaction with EOs. These instability windows for a particular case of $\beta_L = 1$ are shown in Fig. 13. The breather instabilities manifest themselves by various features in the I–V characteristics. For exam-

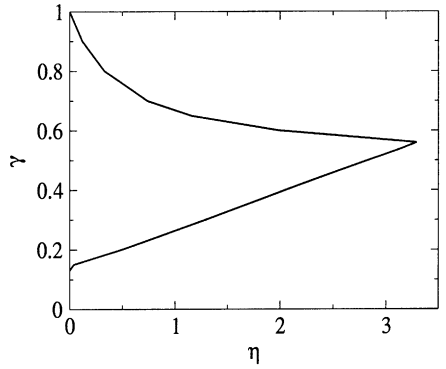

Fig. 12. Domain of breather existence in parameter space (γ, η) for $\beta_L = 100$ and $\alpha = 0.1$.

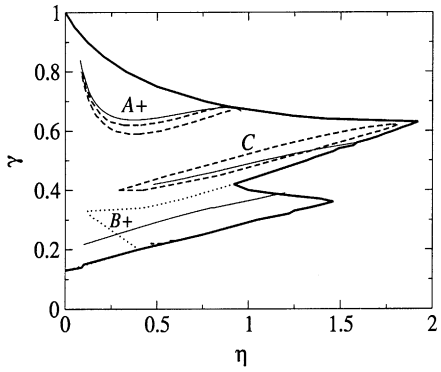

Fig. 13. Domain of breather existence and instability windows (dashed line) in parameter space (γ, η) for $\beta_L = 1$ and $\alpha = 0.1$. The predicted resonances between the breather state and EOs are shown by the thin solid lines. The boundary of the primary resonance is shown by the dotted line.

ple, at the value of anisotropy $\eta = 0.5$, we observed a rich set of resonant steps and voltage jumps in the I–V curve (Fig. 14).

For large values of the d.c. bias ($\gamma \simeq 0.6$), a parametric resonance of the breather state with high frequency EOs, $\Omega = 2\omega_+$ leads to a resonant step in the I–V curve. Moreover, the breather state biased to this resonance displays a period doubling bifurcation which manifests through a sharp corner in the I–V curve at the bottom of the resonant step (A+ region). As the d.c. bias decreases to the value $\gamma \simeq 0.4$, we observe the combination resonance $\Omega = \omega_+ + \omega_-$. This resonance is characterized by a large back bending of the I–V curve and the breather state dynamics displays a *nonperiodic* behaviour (see inset in Fig. 14 and C region).

As the d.c. bias decreases further to the value of $\gamma \simeq 0.37$, a large resonant step in the I–V curve appears. It corresponds to the primary resonance with $\Omega = \omega_+$. This resonant breather state switches to the SS at the value of $\gamma = 0.27$ as a result of an instability driven by the parametric resonance with low frequency EOs, $\Omega = 2\omega_-$ (A region). These features are clearly seen in the dependence of Floquet multipliers on the d.c. bias (see Fig. 15). The type of resonance can be easily detected from the behaviour of the arguments of the Floquet multipliers. While unstable solutions (with absolute values of multipliers being larger than

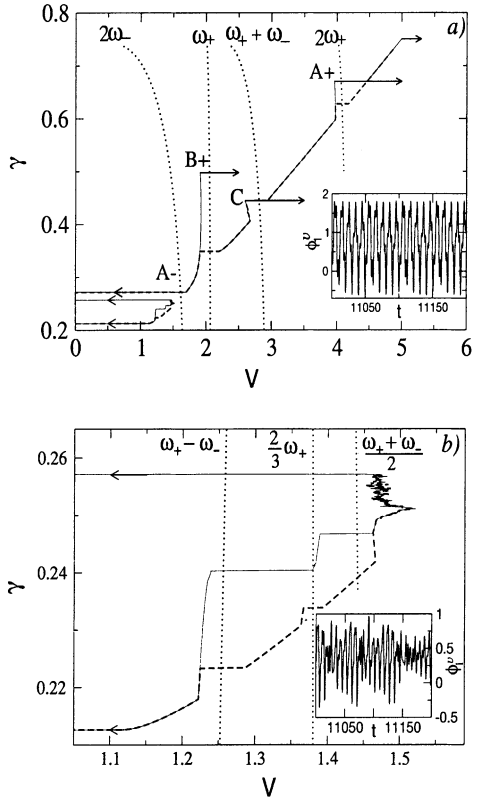

Fig. 14. (a) I–V characteristics of a breather state for $\beta_L = 1$, $\alpha = 0.1$ and $\eta = 0.5$. Thick dashed lines correspond to lowering of the d.c. bias, thin solid lines to an increasing of the d.c. bias. The labels A−, A+, B+ and C relate the resonances to the observed instability windows in Fig. 13. (b) A zoom of the I–V curve. The dependencies of EOs characteristic frequency combinations on the d.c. bias γ are shown by dotted lines. The arrows show the various switching outcomes as the d.c. bias increases (decreases). The time dependence of the Josephson phase ϕ_1^{v} at $\gamma = 0.44$, $V = 2.61$ and $\gamma = 0.25$, $V = 1.482$ are shown as insets.

1), which corresponding to parametric resonances are characterized by 'frozen' arguments at value π, combination resonances are characterized by a merging of arguments over a particular interval of d.c. bias.

For even smaller values of the d.c. bias, namely $0.21 < \gamma < 0.26$, the breather state becomes again stable. For $\gamma \simeq 0.26$, this breather state shows up with a nonperiodic behaviour (see inset in Fig. 14b). Most importantly, we observe three new resonances: a combination resonance $\Omega = \omega_+ - \omega_-$, a parametric resonance $\Omega = \frac{2}{3}\omega_+$ and yet another combination

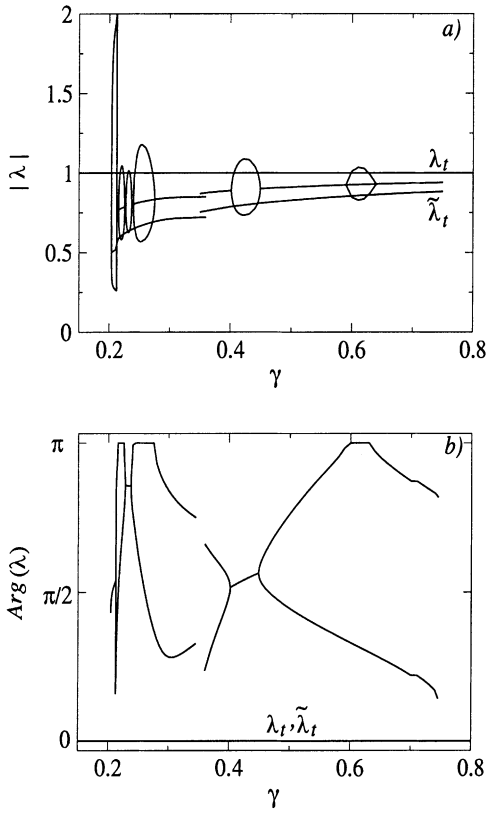

Fig. 15. (a) Modulus and (b) argument of the Floquet multipliers as a function of d.c. bias γ. The parameters are $\beta_L = 1$, $\alpha = 0.1$ and $\eta = 0.5$.

resonance $2\Omega = \omega_+ + \omega_-$. The breather finally switches to the SS at $\gamma = 0.21$.

4. Conclusion

We have presented an analytical and numerical study of inhomogeneous dynamic states (breathers) in a single plaquette consisting of three small underdamped Josephson junctions. We found that as the damping α is small the breather state as a solution of dynamic equations exists in a large region of parameters: d.c. bias γ and anisotropy η (Figs. 2, 3, 12 and 13). For small and moderate values of anisotropy η ($\eta \leq 1$), the d.c. analysis that completely neglects the breather induced EOs (Eqs. (6)–(13)), results in a good estimation of the boundary of breather existence. However, we found that the domain of the breather existence shrinks as the anisotropy η increases, and moreover, for moderate values of the self-inductance β_L, the upper part of the boundary displays a sawtooth feature. These effects are due to the excitation of EOs with large amplitudes.

The second major result of the presence of EOs is that the domain of the breather existence contains a large number of *instability regions*. The physical origin of these instabilities is the resonant interaction between the breather state and the EOs. It is important that due to the presence of two different characteristic frequencies of EOs (for the dependence of $\omega_\pm$ on the self-inductance and anisotropy, see Eq. (18)), a rich set of resonances (primary, parametric or combination ones) occurs. Such resonant interactions can completely destroy the breather state and correspondingly lead to significant shifts of the switchings of the breather state to the HWS or the SS. These switchings appear through voltage jumps in the I–V curves. Note here that in most cases, we observed the switching to the SS as a result of breather instability (parametric or combination), but not due to the standard retrapping mechanism (Eq. (12)). Similar findings have also been reported for large Josephson junction ladders [21].

The most interesting observation is that the breather state can survive the resonant instabilities by increasing its dynamic complexity. This dynamic complexity manifests itself by resonant steps of various types in the I–V curves. Indeed, we observed a *resonant* type breather as a result of a primary resonance with EOs (B+ region in Fig. 14a), a period doubling process resulting from the parametric resonant interaction (Fig. 5, regions A+, A− in Fig. 14) and even a nonperiodic (quasiperiodic or chaotic) behaviour in parameter regions where combination resonances appear (C region and the region of small current in Fig. 14).

Finally, all observed effects (switching outcomes, instabilities) are very sensitive to the damping parameter α, and different combinations of the resonances can appear as the damping parameter α decreases.

Experimental studies will require a different way of generating breather states, as there is in general no control over the initial conditions. A standard way is to inject an additional local current through one of the

two vertical junctions. We verified that the following procedure leads to the generation of breathers starting from the SS: increase a local current through, e.g. the left vertical junction above the critical value and obtain a breather-like state. Decrease this local current below its critical value. The breather-like state still persists. Finally, increase the current through the right vertical junction to the same value. The breather state will survive and we end up with a homogeneous d.c. bias flowing through the two vertical junctions.

It is worthwhile to note that an additional magnetic field perpendicular to the plaquette can significantly alter the observed resonance patterns. In a forthcoming work, we will show that one can use the magnetic field in order to control the strength of resonant interaction. This allows to enhance or suppress resonance features in the I–V curves.

What can we learn about breather states in extended ladder geometries? Our analysis shows that stable breathers can be induced for large self-inductance. If, on the other hand, one needs switchings between different breather states and resonances, intermediate β_L values should be chosen. In addition, variations of the damping (e.g. via temperature control) may increase the complexity of expected switching scenarios. At the same time, it should be clear that if already such a small system (with three degrees of freedom) shows up with a high complexity of the phase space structure, the situation for large number of degrees of freedom as for Josephson ladders will be even more complex.

Acknowledgements

We thank J.J. Mazo, A. Miroshnichenko, J. Page, M. Schuster, A. Ustinov and Y. Zolotaryuk for useful discussions. This work was supported by the European Union under the RTN project LOCNET HPRN-CT-1999-00163.

References

[1] S. Aubry, Physica D 103 (1997) 201.
[2] S. Flach, C.R. Willis, Phys. Rep. 295 (1998) 182.
[3] A.J. Sievers, J.B. Page, in: G.K. Horton, A.A. Maradudin (Eds.), Dynamical Properties of Solids, VII: Phonon Physics, Elsevier, Amsterdam, 1995.
[4] H.S. Eisenberg, Y. Silberberg, R. Morandotti, A.R. Boyd, J.S. Aitchison, Phys. Rev. Lett. 81 (1998) 3383.
[5] B.I. Swanson, J.A. Brozik, S.P. Love, G.F. Strouse, A.P. Shreve, A.R. Bishop, W.-Z. Wang, M.I. Salkola, Phys. Rev. Lett. 82 (1999) 3288.
[6] U.T. Schwarz, L.Q. English, A.J. Sievers, Phys. Rev. Lett. 83 (1999) 223.
[7] E. Trías, J.J. Mazo, T.P. Orlando, Phys. Rev. Lett. 84 (2000) 741.
[8] P. Binder, D. Abraimov, A.V. Ustinov, S. Flach, Y. Zolotaryuk, Phys. Rev. Lett. 84 (2000) 745.
[9] P. Binder, D. Abraimov, A.V. Ustinov, Phys. Rev. E 62 (2000) 2858.
[10] E. Trías, J.J. Mazo, A. Brinkman, T.P. Orlando, Physica D 156 (2001) 98.
[11] M. Schuster, P. Binder, A.V. Ustinov, Phys. Rev. E, submitted.
[12] L.M. Floria, J.L. Marin, P.L. Martínez, F. Falo, S. Aubry, Europhys. Lett. 36 (1996) 539.
[13] P.J. Martínez, L.M. Floría, S. Aubry, J.J. Mazo, Physica D 119 (1998) 175.
[14] S. Flach, M. Spicci, J. Phys. Condens. Matter 11 (1999) 321.
[15] J.J. Mazo, E. Trías, T.P. Orlando, Phys. Rev. B 59 (1999) 13604.
[16] D. Abraimov, P. Caputo, G. Filatrella, M.V. Fistul, G.Yu. Logvenov, A.V. Ustinov, Phys. Rev. Lett. 83 (1999) 5354.
[17] K.K. Likharev, Dynamics of Josephson Junctions and Circuits, Gordon and Breach, Pennsylvania, PA, 1986.
[18] A. Barone, G. Paterno, Physics and Applications of the Josephson Effect, Wiley, New York, 1982.
[19] R.S. MacKay, J.-A. Sepulchre, Physica D 119 (1998) 148.
[20] V.I. Arnold, Mathematical Methods of Classical Mechanics, Springer, Berlin, 1989.
[21] A.E. Miroshnichenko, S. Flach, M.V. Fistul, Y. Zolotaryuk, J.B. Page, Phys. Rev. E, in press, cond-mat 0103280.
[22] M.V. Fistul, A.V. Ustinov, Phys. Rev. B 63 (2001) 024508.